Simultaneous Schur Decomposition of Several Nonsymmetric Matrices to Achieve Automatic Pairing in Multidimensional Harmonic Retrieval Problems

Martin Haardt, *Member, IEEE,* and Josef A. Nossek, *Fellow, IEEE*

***Abstract*— This paper presents a new Jacobi-type method to calculate a simultaneous Schur decomposition (SSD) of several real-valued, nonsymmetric matrices by minimizing an appropriate cost function. Thereby, the SSD reveals the "average eigenstructure" of these nonsymmetric matrices. This enables an R-dimensional extension of Unitary ESPRIT to estimate several undamped R-dimensional modes or frequencies along with their correct pairing in multidimensional harmonic retrieval problems. Unitary ESPRIT is an ESPRIT-type high-resolution frequency estimation technique that is formulated in terms of real-valued computations throughout. For each of the R dimensions, the corresponding frequency estimates are obtained from the real eigenvalues of a real-valued matrix. The SSD jointly estimates the eigenvalues of all R matrices and, thereby, achieves automatic pairing of the estimated R-dimensional modes via a closed-form procedure that neither requires any search nor any other heuristic pairing strategy. Moreover, we describe how R-dimensional harmonic retrieval problems (with $R \geq 3$) occur in array signal processing and model-based object recognition applications.**

***Index Terms*—Array signal processing, direction-of-arrival estimation, eigenvalues, frequency estimation, harmonic analysis, linear algebra, multidimensional sequences, multidimensional signal processing, object recognition, planar arrays, radar, smooting methods.**

I. Introduction

DUE to its simplicity and high-resolution capability, *ESPRIT* has become one of the most popular subspace-based direction of arrival or frequency estimation schemes. For certain array geometries, namely centro-symmetric arrays, or undamped modes in the frequency domain, the computational complexity can be reduced significantly by formulating an ESPRIT-type algorithm in terms of real-valued computations throughout. The resulting algorithm is called *Unitary ESPRIT*, since the estimated phase factors are automatically constrained to the unit circle [9]. Furthermore, Unitary ESPRIT has recently been extended to the two-dimensional (2-D) case to provide automatically paired azimuth and elevation angle estimates [6], [20]. If, however, the carrier frequencies of the impinging wavefronts are no longer known (e.g., due to Doppler shifts) and may differ, the 2-D arrival angles, azimuth and elevation, and the corresponding carrier frequencies have to be estimated simultaneously. This model applies, for instance, to the surveillance radar system discussed in [18] and requires a three-dimensional (3-D) extension of Unitary ESPRIT. Moreover, *3-D Unitary ESPRIT for joint 2-D angle and carrier estimation* can be used to determine the 2-D arrival angles, frequency offsets, and damping factors of the dominant multipaths in an SDMA (space division multiple access) mobile radio system [11]. Here, 3-D Unitary ESPRIT can provide precise 2-D arrival angle estimates even if only a small number of antennas is available.

In [14] and [15] it was shown how the parameters of certain statistical mobile radio channel models can be obtained from the results of field propagation measurements. The author described a measurement setup (channel sounder) where high-resolution estimates of the propagation path delays were determined in the frequency domain by solving the one-dimensional (1-D) harmonic retrieval problem. Obviously, 1-D Unitary ESPRIT could also be used for this task. After replacing the receiving antenna of this channel sounder by a uniform rectangular array (URA) of identical antennas, 3-D Unitary ESPRIT can provide automatically paired 2-D arrival angle and delay estimates of the dominant propagation paths. Such high-resolution directional measurements of the mobile radio channel facilitate the development of realistic directional channel models that include 2-D directions of arrival, namely azimuth and elevation angles. In several field experiments conducted by Deutsche Telekom AG, 2-D Unitary ESPRIT has already been used successfully in conjunction with this channel sounder and a uniform linear array (ULA) to provide automatically paired 1-D arrival angle and delay estimates of the dominant propagation paths. Preliminary measurement results have been reported in [16].

To give another application, assume that the usual plane wave approximation of the impinging wavefronts is no longer accurate since a uniform rectangular array is located in the *Fresnel* region or the *near-field* of the sources. Then 3-D Unitary ESPRIT can be applied to certain fourth-order cross-cumulant matrices to estimate the 2-D arrival angles and ranges of several near-field sources simultaneously. This task

Manuscript received November 26, 1996; revised June 18, 1997. The associate editor coordinating the review of this paper and approving it for publication was Barry D. Van Veen.

M. Haardt is with Siemens AG, OEN MN P 36, D-81359 Munich, Germany (e-mail: martin.haardt@oen.siemens.de).

J. A. Nossek is with the Institute of Network Theory and Circuit Design, Technical University of Munich, D-80290 Munich, Germany (e-mail: nossek@nws.e-technik.tu-muenchen.de).

Publisher Item Identifier S 1053-587X(98)00511-X.

may be achieved via straightforward 3-D extensions of the 2-D Unitary ESPRIT based algorithms for (passive) near-field source localization presented in [8].

Furthermore, the model-based object recognition scheme presented in [1], [4], and [19] provides another application of the multidimensional harmonic retrieval problem. Here, the generated measurements correspond to samples from an R-dimensional lattice of sensors. These synthetic waveform samples are obtained from an image by applying certain reciprocal basis functions, which were generated (off-line) from a sequence of object views [4], [19]. In this application, R denotes the number of pose parameters that can easily exceed three. These pose parameters may include six orientation parameters (the object's location in space and the corresponding three Euler angles of rotation) and also parameters describing other variable characteristics, e.g., the relative position of articulated components of the object [19]. Then the estimated R-dimensional undamped modes are the parameters that reveal the object identities and their orientations. In this context, R-D Unitary ESPRIT provides an efficient way to find the identities and poses of *several* (d) objects within a single image simultaneously. Notice that the R estimated parameters per object will be automatically paired which facilitates an efficient extension of the work presented in [4].[1]

This paper is organized as follows. After introducing the data model of the multidimensional harmonic retrieval problem in Section II-A, we describe the multidimensional extension of Unitary ESPRIT in Section II-B. In Section II-C, the 1-D smoothing concept known from array signal processing is extended to the R-dimensional case to be used as a preprocessing step for R-D Unitary ESPRIT. Then the simultaneous Schur decomposition (SSD) of several real-valued nonsymmetric matrices is introduced in Section III. An efficient Jacobi-type algorithm to calculate the SSD is presented in Section III-B. As a 3-D application, we consider 3-D Unitary ESPRIT for joint 2-D angle and carrier estimation in Section IV. Simulation examples that illustrate the performance of 3-D Unitary ESPRIT and the SSD are presented at the end of the same section, before Section V concludes the paper.

Notation: Let us begin by introducing our notation. Throughout this paper, column vectors and matrices are denoted by lower-case and upper-case boldfaced letters, respectively. For any positive integer p, $\boldsymbol{I}_p$ denotes the $p \times p$ identity matrix and $\boldsymbol{\Pi}_p$ the $p \times p$ exchange matrix with ones on its antidiagonal and zeros elsewhere, as follows:

$$\boldsymbol{\Pi}_p = \begin{bmatrix} & & 1 \\ & \iddots & \\ 1 & & \end{bmatrix} \in \mathbb{R}^{p \times p}.$$

Furthermore, the superscripts $(\cdot)^H$ and $(\cdot)^T$ denote complex conjugate transposition and transposition without complex conjugation, respectively. Complex conjugation by itself is denoted by an overbar $\overline{(\cdot)}$, such that $\boldsymbol{X}^H = \overline{\boldsymbol{X}}^T$. Finally, a diagonal matrix $\boldsymbol{\Phi}$ with the diagonal elements $\phi_1, \phi_2, \cdots, \phi_d$ may be written as

$$\boldsymbol{\Phi} = \operatorname{diag}\{\phi_i\}_{i=1}^{d} = \begin{bmatrix} \phi_1 & & & \\ & \phi_2 & & \\ & & \ddots & \\ & & & \phi_d \end{bmatrix} \in \mathbb{C}^{d \times d}.$$

II. Multidimensional Harmonic Retrieval

A. Data Model

Suppose we conduct N trials or experiments to observe noise-corrupted measurements $x_{k_1,k_2,\cdots,k_R}(n)$ on an R-dimensional lattice[2] for $1 \le n \le N$. The index of the rth dimension k_r is allowed to vary from 0 to $(M_r - 1)$ for $1 \le r \le R$. Thus, for fixed n, we have

$$M = \prod_{r=1}^{R} M_r$$

different measurements of the data. This R-dimensional data consists of d undamped exponential modes in additive noise

$$x_{k_1,k_2,\cdots,k_R}(n) = \sum_{i=1}^{d} \left[s_i(n) \prod_{r=1}^{R} e^{\mathrm{j}\mu_i^{(r)} k_r} \right] + n_{k_1,k_2,\cdots,k_R}(n) \tag{1}$$

where the additive noise process is assumed to be zero-mean, i.i.d., with variance σ_N^2, and uncorrelated with the signals. Here, we consider the task of estimating the d frequency vectors

$$\boldsymbol{\mu}_i = [\mu_i^{(1)} \quad \mu_i^{(2)} \quad \cdots \quad \mu_i^{(R)}]^T \qquad 1 \le i \le d \tag{2}$$

that correspond to the d R-dimensional modes and their correct pairing from the noise-corrupted measurements in (1). Observe that equation (1) represents a straightforward R-dimensional extension of the familiar 1-D and 2-D harmonic retrieval problems.

B. Multidimensional Extension of Unitary ESPRIT

A very simple and efficient way to achieve this goal would be an R-dimensional extension of *Unitary ESPRIT*. As in the 1-D case [9], the algorithm is formulated in terms of real-valued computations throughout due to a bijective mapping between centro-Hermitian and real matrices [13], which automatically achieves forward–backward averaging of the data. Without loss of generality, we only describe the *element space implementation* of R-D Unitary ESPRIT. If one desires to operate in a lower dimensional beamspace to focus on a particular sector of interest, an R-dimensional extension of *Unitary ESPRIT in DFT beamspace* [20] can be obtained in a similar fashion.

[1] In [4], the authors propose an algorithm to identify the identity and orientation of a single object, i.e., $d = 1$.

[2] In this paper, we develop R-D Unitary ESPRIT for measurements taken on the Cartesian product of R uniform linear grids (arrays). The same algorithm, however, can also be applied to more general lattice geometries, namely to all lattices that are centro-symmetric and exhibit an R-dimensional invariance structure, cf., [6] for a discussion of the corresponding 2-D case.

First of all, measurement vectors

$$\boldsymbol{x}(n) = \begin{bmatrix} x_{0,0,\cdots,0}(n) \\ x_{1,0,\cdots,0}(n) \\ \vdots \\ x_{M_1-1,0,\cdots,0}(n) \\ x_{M_1-1,1,\cdots,0}(n) \\ \vdots \\ x_{M_1-1,M_2-1,\cdots,M_R-2}(n) \\ x_{M_1-1,M_2-1,\cdots,M_R-1}(n) \end{bmatrix} \in \mathbb{C}^M \tag{3}$$

are formed from the scalar measurements in (1). These measurement vectors $\boldsymbol{x}(n)$, $1 \le n \le N$, are placed as columns of a data matrix $\boldsymbol{X} \in \mathbb{C}^{M\times N}$. If only a single vector $\boldsymbol{x}(n)$ is available ($N = 1$), R-dimensional smoothing as described at the end of this section should be used to "create" more snapshots artificially. It is straightforward to show that the data matrix $\boldsymbol{X}$ satisfies the linear model

$$\begin{aligned} \boldsymbol{X} &= [\boldsymbol{x}(1) \quad \boldsymbol{x}(2) \quad \cdots \quad \boldsymbol{x}(N)] \\ &= \boldsymbol{A}[\boldsymbol{s}(1) \quad \boldsymbol{s}(2) \quad \cdots \quad \boldsymbol{s}(N)] \\ &\quad + [\boldsymbol{n}(1) \quad \boldsymbol{n}(2) \quad \cdots \quad \boldsymbol{n}(N)] \end{aligned} \tag{4}$$

where the vectors $\boldsymbol{s}(n) \in \mathbb{C}^d$ and $\boldsymbol{n}(n) \in \mathbb{C}^M$ contain the corresponding signal and noise samples. Furthermore, the columns of the steering matrix $\boldsymbol{A} \in \mathbb{C}^{M\times d}$ can be written as Kronecker products of the Vandermonde vectors

$$\boldsymbol{a}(\mu_i^{(r)}) = [1 \quad e^{\mathrm{j}\mu_i^{(r)}} \quad e^{\mathrm{j}2\mu_i^{(r)}} \quad \cdots \quad e^{\mathrm{j}(M_r-1)\mu_i^{(r)}}]^T \in \mathbb{C}^{M_r}$$

namely

$$\begin{aligned} \boldsymbol{a}(\mu_i^{(1)}, \mu_i^{(2)}, \cdots, \mu_i^{(R)}) &= \boldsymbol{a}(\mu_i^{(R)}) \otimes \boldsymbol{a}(\mu_i^{(R-1)}) \otimes \cdots \otimes \boldsymbol{a}(\mu_i^{(2)}) \\ &\quad \otimes \boldsymbol{a}(\mu_i^{(1)}), \qquad 1 \le i \le d. \end{aligned} \tag{5}$$

Then we define R pairs of selection matrices of size $m_r \times M$, $1 \le r \le R$, that are centro-symmetric with respect to one another, i.e.,

$$\boldsymbol{J}_{(r)1} = \boldsymbol{\Pi}_{m_r} \boldsymbol{J}_{(r)2} \boldsymbol{\Pi}_M \text{ with} \tag{6}$$

$$m_r = (M_r - 1) \prod_{\substack{k=1 \\ k\neq r}}^{R} M_k = \frac{M(M_r-1)}{M_r}, \qquad 1 \le r \le R$$

and cause the multidimensional steering vectors (5) to satisfy the following invariance properties:

$$\begin{aligned} &\boldsymbol{J}_{(r)1}\boldsymbol{a}(\mu_i^{(1)}, \mu_i^{(2)}, \cdots, \mu_i^{(R)}) \cdot e^{\mathrm{j}\mu_i^{(r)}} = \\ &\quad \boldsymbol{J}_{(r)2}\boldsymbol{a}(\mu_i^{(1)}, \mu_i^{(2)}, \cdots, \mu_i^{(R)}), \qquad 1 \le i \le d, \quad 1 \le r \le R. \end{aligned}$$

In matrix notation, these invariance properties may be summarized as

$$\boldsymbol{J}_{(r)1}\boldsymbol{A} \cdot \boldsymbol{\Phi}_r = \boldsymbol{J}_{(r)2}\boldsymbol{A}, \qquad 1 \le r \le R \tag{7}$$

where the R diagonal matrices

$$\boldsymbol{\Phi}_r = \mathrm{diag}\{e^{\mathrm{j}\mu_i^{(r)}}\}_{i=1}^d$$

contain the phase factors. To give an explicit formula for the multidimensional selection matrices, define

$$\boldsymbol{J}_2^{(M_r)} = [\boldsymbol{0}_{(M_r-1)\times 1} \quad \boldsymbol{I}_{M_r-1}]$$

as a 1-D selection matrix corresponding to maximum overlap in the rth direction. Here, $\boldsymbol{0}_{(M_r-1)\times 1}$ denotes the zero matrix of size $(M_r - 1) \times 1$. Taking into account the described R-dimensional stacking procedure, we can construct the desired $m_r \times M$ dimensional selection matrices as

$$\begin{aligned} \boldsymbol{J}_{(r)2} &= (\boldsymbol{I}_{M_R} \otimes \boldsymbol{I}_{M_{R-1}} \otimes \cdots \otimes \boldsymbol{I}_{M_{r+1}}) \otimes \boldsymbol{J}_2^{(M_r)} \\ &\quad \otimes (\boldsymbol{I}_{M_{r-1}} \otimes \cdots \otimes \boldsymbol{I}_{M_1}) \\ &= \boldsymbol{I}_{\prod_{k=(r+1)}^{R} M_k} \otimes \boldsymbol{J}_2^{(M_r)} \otimes \boldsymbol{I}_{\prod_{k=1}^{r-1} M_k} \qquad 1 \le r \le R. \end{aligned}$$

As a simple example, consider the case $R = 3$. According to the previous discussion, we have

$$\begin{aligned} \boldsymbol{J}_{(1)2} &= \boldsymbol{I}_{M_3} \otimes \boldsymbol{I}_{M_2} \otimes \boldsymbol{J}_2^{(M_1)} = \boldsymbol{I}_{M_2M_3} \otimes \boldsymbol{J}_2^{(M_1)} \\ \boldsymbol{J}_{(2)2} &= \boldsymbol{I}_{M_3} \otimes \boldsymbol{J}_2^{(M_2)} \otimes \boldsymbol{I}_{M_1} \\ \boldsymbol{J}_{(3)2} &= \boldsymbol{J}_2^{(M_3)} \otimes \boldsymbol{I}_{M_2} \otimes \boldsymbol{I}_{M_1} = \boldsymbol{J}_2^{(M_3)} \otimes \boldsymbol{I}_{M_1M_2}. \end{aligned}$$

If desired, the selection matrices $\boldsymbol{J}_{(r)1}$, $r = 1,2,3$, can be obtained from (6). In fact, to be able to compute the $2R = 6$ transformed selection matrices required for R-D Unitary ESPRIT as summarized in Table I, it is sufficient to specify $\boldsymbol{J}_{(1)2}$, $\boldsymbol{J}_{(2)2}$, and $\boldsymbol{J}_{(3)2}$, cf., (10).

Real-Valued Invariance Equations: Let left $\boldsymbol{\Pi}$-real matrices be defined as matrices $\boldsymbol{Q} \in \mathbb{C}^{M\times M}$ satisfying $\boldsymbol{\Pi}_M\overline{\boldsymbol{Q}} = \boldsymbol{Q}$ [9], [13]. The unitary matrix

$$\boldsymbol{Q}_{2q+1} = \frac{1}{\sqrt{2}} \begin{bmatrix} \boldsymbol{I}_q & \boldsymbol{0} & \mathrm{j}\boldsymbol{I}_q \\ \boldsymbol{0}^T & \sqrt{2} & \boldsymbol{0}^T \\ \boldsymbol{\Pi}_q & \boldsymbol{0} & -\mathrm{j}\boldsymbol{\Pi}_q \end{bmatrix} \tag{8}$$

for example, is left $\boldsymbol{\Pi}$-real of odd order. A unitary left $\boldsymbol{\Pi}$-real matrix of size $2q \times 2q$ is obtained from (8) by dropping its center row and center column. More left $\boldsymbol{\Pi}$-real matrices can be constructed by postmultiplying a left $\boldsymbol{\Pi}$-real matrix $\boldsymbol{Q}$ by an arbitrary real matrix $\boldsymbol{R}$, i.e., every matrix $\boldsymbol{QR}$ is left $\boldsymbol{\Pi}$-real.

As in the 2-D case [20], let us define the transformed steering matrix as $\boldsymbol{D} = \boldsymbol{Q}_M^H\boldsymbol{A}$. Based on the R invariance properties of the multidimensional steering matrix $\boldsymbol{A}$ in (7), it is a straightforward R-D extension of the derivation of 1-D and 2-D Unitary ESPRIT to show that the transformed array steering matrix $\boldsymbol{D}$ satisfies

$$\boldsymbol{K}_{(r)1}\boldsymbol{D} \cdot \boldsymbol{\Omega}_r = \boldsymbol{K}_{(r)2}\boldsymbol{D}, \qquad 1 \le r \le R \tag{9}$$

where the R corresponding pairs of transformed selection matrices are given by

$$\boldsymbol{K}_{(r)1} = 2 \cdot \mathrm{Re}\{\boldsymbol{Q}_{m_r}^H \boldsymbol{J}_{(r)2} \boldsymbol{Q}_M\}$$

and

$$\boldsymbol{K}_{(r)2} = 2 \cdot \mathrm{Im}\{\boldsymbol{Q}_{m_r}^H \boldsymbol{J}_{(r)2} \boldsymbol{Q}_M\} \tag{10}$$

and the R real-valued diagonal matrices

$$\boldsymbol{\Omega}_r = \mathrm{diag}\left\{ \tan\left[\frac{\mu_i^{(r)}}{2}\right] \right\}_{i=1}^{d}, \qquad 1 \le r \le R \tag{11}$$

contain the desired frequency information.

In the first step of Unitary ESPRIT [6], [20], forward–backward averaging is achieved by transforming the complex-valued data matrix $\boldsymbol{X}$ into the real-valued matrix[3]

$$\mathcal{T}(\boldsymbol{X}) = \boldsymbol{Q}_M^H [\boldsymbol{X} \quad \boldsymbol{\Pi}_M \overline{\boldsymbol{X}} \boldsymbol{\Pi}_N] \boldsymbol{Q}_{2N} \in \mathbb{R}^{M \times 2N}.$$

Its d dominant left singular vectors $\boldsymbol{E}_s \in \mathbb{R}^{M \times d}$ are determined through a real-valued SVD of $\mathcal{T}(\boldsymbol{X})$ (square-root approach). Alternatively, they can be computed through a real-valued eigendecomposition of $\mathcal{T}(\boldsymbol{X})\mathcal{T}(\boldsymbol{X})^H \in \mathbb{R}^{M \times M}$ (covariance approach). Asymptotically or without additive noise, $\boldsymbol{E}_s$ and $\boldsymbol{D}$ span the same d-dimensional subspace, i.e., there is a nonsingular matrix $\boldsymbol{T}$ of size $d \times d$ such that $\boldsymbol{D} \approx \boldsymbol{E}_s \boldsymbol{T}$. Substituting this relationship into (9) yields R *real-valued* invariance equations

$$\boldsymbol{K}_{(r)1} \boldsymbol{E}_s \boldsymbol{\Upsilon}_r \approx \boldsymbol{K}_{(r)2} \boldsymbol{E}_s \in \mathbb{R}^{m_r \times d}, \text{ where } \boldsymbol{\Upsilon}_r = \boldsymbol{T} \boldsymbol{\Omega}_r \boldsymbol{T}^{-1} \quad 1 \le r \le R. \tag{12}$$

Thus, the R real-valued matrices $\boldsymbol{\Upsilon}_r$ are related with the diagonal matrices $\boldsymbol{\Omega}_r$ via eigenvalue preserving similarity transformations. Moreover, they share the *same set of eigenvectors* $\boldsymbol{T}$. As in the 2-D case, the R invariance equations (12) can be solved independently via least squares (LS), total least squares (TLS), or structured least squares (SLS) [7] or jointly via an R-dimensional extension of SLS (R-D SLS), yielding R real-valued matrices $\boldsymbol{\Upsilon}_r \in \mathbb{R}^{d \times d}$, $1 \le r \le R$. Note that these matrices are not necessarily symmetric.

In the noiseless case or with an infinite number of experiments N, the real-valued eigenvalues of the solutions $\boldsymbol{\Upsilon}_r \in \mathbb{R}^{d \times d}$ to the R invariance equations above are given by $\tan[\mu_i^{(r)}/2]$. If these eigenvalues were calculated independently, it would be quite difficult to pair the resulting R distinct sets of frequency estimates. Notice that one can choose a real-valued eigenvector matrix $\boldsymbol{T}$ such that all matrices that appear in the spectral decompositions of $\boldsymbol{\Upsilon}_r = \boldsymbol{T} \boldsymbol{\Omega}_r \boldsymbol{T}^{-1}$ are real-valued. If the matrix of eigenvectors $\boldsymbol{T} \in \mathbb{R}^{d \times d}$ is the same for all r, $1 \le r \le R$, the diagonal elements of the matrices $\boldsymbol{\Omega}_r$ and, therefore, also the corresponding frequencies are automatically paired. These observations are critical to achieve automatic pairing of the estimated frequencies $\mu_i^{(r)}$, $1 \le i \le d$, $1 \le r \le R$.

In practice, though, only a finite number N of noise-corrupted experiments (or measurements) is available. Therefore, the R matrices $\boldsymbol{\Upsilon}_r$ do not exactly share the same set of eigenvectors. To determine an approximation of the set of common eigenvectors only from one of the $\boldsymbol{\Upsilon}_r$ is, obviously, not the best solution, since this strategy would rely on an arbitrary choice and would also discard information contained in the other $R-1$ matrices. Moreover, each of the $\boldsymbol{\Upsilon}_r$ might have some degenerate (multiple) eigenvalues, while the whole set $\boldsymbol{\Upsilon}_r$, $1 \le r \le R$, has well-determined common eigenvectors $\boldsymbol{T}$ (for $N \to \infty$ or $\sigma_N^2 \to 0$). Thus, from a statistical point of view, it is desirable, for the sake of accuracy and robustness, to compute the "average eigenstructure" of these matrices [3]. In the 2-D case, this problem was solved by calculating the eigenvalues of the "complexified" matrix $\boldsymbol{\Upsilon}_1 + j\boldsymbol{\Upsilon}_2 \in \mathbb{C}^{d \times d}$, as discussed in [6] and [20]. Thereby, automatic pairing of the eigenvalues can be achieved. If, however, $R > 2$, this "trick" has to be extended to the R-dimensional case. To this end, we develop a Jacobi-type method to calculate an SSD of several nonsymmetric matrices.

[3] If the left $\boldsymbol{\Pi}$-real matrices $\boldsymbol{Q}_M$ and $\boldsymbol{Q}_{2N}$ are chosen according to (8) and M is even, an efficient computation of the transformation $\mathcal{T}(\boldsymbol{X}) \in \mathbb{R}^{M \times 2N}$ from the complex-valued data matrix $\boldsymbol{X}$ only requires $M \cdot 2N$ real additions and no multiplication [9].

C. R-Dimensional Smoothing as a Preprocessing Step for R-D Unitary ESPRIT

Before presenting the SSD in Section III, let us briefly extend the 2-D smoothing concept of [10] to the R-dimensional case. If only one trial or experiment is available ($N = 1$), R-dimensional smoothing should, for instance, be used as a preprocessing step for the multidimensional extension of Unitary ESPRIT summarized in Table I. Note that 1-D smoothing could be applied to each of the R dimensions independently by dividing the M_r measurements of the rth dimension into L_r groups (or subarrays), each containing $M_{\text{sub}_r} = M_r - L_r + 1$ measurements. The corresponding 1-D selection matrices are given by

$$\boldsymbol{J}_{\ell_r}^{(M_r)} = [\boldsymbol{0}_{M_{\text{sub}_r} \times (\ell_r - 1)} \quad \boldsymbol{I}_{M_{\text{sub}_r}} \quad \boldsymbol{0}_{M_{\text{sub}_r} \times (L_r - \ell_r)}] \quad 1 \le \ell_r \le L_r \text{ for } 1 \le r \le R. \tag{13}$$

As a straightforward R-dimensional extension of the 2-D smoothing procedure presented in [10], we define the following $L = \prod_{r=1}^{R} L_r$ multidimensional selection matrices

$$\boldsymbol{J}_{\ell_1, \ell_2, \cdots, \ell_{R-1}, \ell_R} = \boldsymbol{J}_{\ell_R}^{(M_R)} \otimes \boldsymbol{J}_{\ell_{R-1}}^{(M_{R-1})} \otimes \cdots \otimes \boldsymbol{J}_{\ell_2}^{(M_2)} \otimes \boldsymbol{J}_{\ell_1}^{(M_1)} \in \mathbb{R}^{M_{\text{sub}} \times M}, \qquad 1 \le \ell_r \le L_r \tag{14}$$

where $M_{\text{sub}} = \prod_{r=1}^{R} M_{\text{sub}_r}$. Then the smoothed data matrix

$$\boldsymbol{X}_{\text{SS}} = [\boldsymbol{J}_{1,1,\cdots,1,1}\boldsymbol{X} \quad \boldsymbol{J}_{1,1,\cdots,1,2}\boldsymbol{X} \quad \cdots \quad \boldsymbol{J}_{1,1,\cdots,1,L_R}\boldsymbol{X} \quad \boldsymbol{J}_{1,1,\cdots,2,1}\boldsymbol{X} \quad \cdots \quad \boldsymbol{J}_{L_1,L_2,\cdots,L_{R-1},L_R}\boldsymbol{X}]$$

which is of size $M_{\text{sub}} \times NL$, replaces the original data matrix $\boldsymbol{X} \in \mathbb{C}^{M \times N}$ in step 1 of the summary of R-D Unitary ESPRIT (Table I), and the dimensions M, N, and M_r are replaced by M_{sub}, NL, and M_{sub_r}, $1 \le r \le R$, respectively.

III. Simultaneous Schur Decomposition (SSD)

A. Minimization Task

Recall that the real eigenvalues of real-valued nonsymmetric matrices can efficiently be computed through an eigenvalue-revealing real Schur decomposition [5]. In the noiseless case or with an infinite number of experiments N, the new simultaneous Schur decomposition (SSD) of the R matrices $\boldsymbol{\Upsilon}_r$, $1 \le r \le R$, yields R (real-valued) upper triangular matrices that exhibit the automatically paired (real-valued) eigenvalues on their main diagonals. Under the assumption of additive noise and a finite number of experiments N, an orthogonal similarity transformation

TABLE I
SUMMARY OF R-D UNITARY ESPRIT IN ELEMENT SPACE

1. Signal Subspace Estimation: Compute $\boldsymbol{E}_s \in \mathbb{R}^{M\times d}$

- as the d dominant left singular vectors of $\mathcal{T}(\boldsymbol{X}) \in \mathbb{R}^{M\times 2N}$ (square-root approach)
- or the d dominant eigenvectors of $\mathcal{T}(\boldsymbol{X})\mathcal{T}(\boldsymbol{X})^H \in \mathbb{R}^{M\times M}$ (covariance approach).

2. Solution of the Invariance Equations: Then solve

$$\underbrace{\boldsymbol{K}_{(r)1}\boldsymbol{E}_s}_{\mathbb{R}^{m_r\times d}}\boldsymbol{\Upsilon}_r \approx \underbrace{\boldsymbol{K}_{(r)2}\boldsymbol{E}_s}_{\mathbb{R}^{m_r\times d}}, \qquad 1\le r\le R,$$

by means of LS, TLS, SLS, or R-D SLS.

3. Joint Frequency Estimation: Compute the **SSD** of the R real-valued $d\times d$ matrices $\boldsymbol{\Upsilon}_r$ as

$$\boldsymbol{U}_r = \boldsymbol{\Theta}^T\boldsymbol{\Upsilon}_r\boldsymbol{\Theta}, \qquad 1\le r\le R,$$

where $u_{ii}^{(r)}$, $1\le i\le d$, are the diagonal elements of $\boldsymbol{U}_r$.

- $\mu_i^{(r)} = 2\arctan\left(u_{ii}^{(r)}\right), \qquad 1\le i\le d, \qquad 1\le r\le R$

might not be able to produce R upper triangular matrices simultaneously, since the R "noisy" matrices do not share a common set of eigenvectors. In this case, the resulting matrices should be "almost" upper triangular in a least squares sense, i.e., an approximate simultaneous upper triangularization that reveals the "average eigenstructure" should be calculated.

To derive an appropriate algorithm, let $\mathcal{L}(\boldsymbol{\Upsilon}_r)$ denote an operator that extracts the strictly lower triangular part of its matrix-valued argument by setting the upper triangular part and the elements on the main diagonal to zero. Then we want to minimize the cost function

$$\psi(\boldsymbol{\Theta}) = \sum_{r=1}^{R} ||\mathcal{L}(\boldsymbol{\Theta}^T\boldsymbol{\Upsilon}_r\boldsymbol{\Theta})||_{\mathrm{F}}^2 \tag{15}$$

over the set of orthogonal matrices $\boldsymbol{\Theta}\in\mathbb{R}^{d\times d}$ that can be written as products of elementary Jacobi rotations. As usual, $||\cdot||_{\mathrm{F}}$ denotes the Frobenius-norm. The element space implementation of the resulting R-dimensional extension of Unitary ESPRIT is summarized in Table I. If all the $\boldsymbol{\Upsilon}_r$ were symmetric, the minimization of (15) would achieve an approximate simultaneous *diagonalization* of these matrices. An efficient Jacobi-type technique to achieve such an approximate simultaneous diagonalization has been presented in [2] and [3]. This algorithm, however, is not applicable in our case, since the $\boldsymbol{\Upsilon}_r$ are not symmetric. Therefore, the minimization of the sum of the off-diagonal norms of these R matrices via a sequence of simultaneous orthogonal transformations as discussed in [2] and [3] would not reveal the desired "average eigenstructure" of these nonsymmetric matrices.

B. Jacobi-Type Algorithm

In Jacobi-type algorithms, the orthogonal matrix $\boldsymbol{\Theta}$ is decomposed into a product of elementary Jacobi rotations

$$\boldsymbol{\Theta}_{qp} = \begin{bmatrix} 1 & \cdots & 0 & \cdots & 0 & \cdots & 0\\ \vdots & \ddots & \vdots & & \vdots & & \vdots\\ 0 & \cdots & c & \cdots & s & \cdots & 0\\ \vdots & & \vdots & \ddots & \vdots & & \vdots\\ 0 & \cdots & -s & \cdots & c & \cdots & 0\\ \vdots & & \vdots & & \vdots & \ddots & \vdots\\ 0 & \cdots & 0 & \cdots & 0 & \cdots & 1 \end{bmatrix} \tag{16}$$

such that

$$\boldsymbol{\Theta} = \prod_{\#\text{ of sweeps}} \prod_{q=1}^{d}\prod_{p=1}^{q-1} \boldsymbol{\Theta}_{qp}. \tag{17}$$

Jacobi rotations $\boldsymbol{\Theta}_{qp}$ are defined as orthogonal matrices where all diagonal elements are one except for the two elements c in rows (and columns) p and q. Likewise, all off-diagonal elements of $\boldsymbol{\Theta}_{qp}$ are zero except for the two elements s and $-s$, cf., (16). The real numbers $c=\cos\vartheta$ and $s=\sin\vartheta$ are the cosine and sine of a rotation angle ϑ such that $c^2+s^2=1$. In the sequel, we describe a procedure to choose the rotation angle ϑ at a particular iteration such that the cost function $\psi(\boldsymbol{\Theta})$ is decreased as much as possible. To this end, observe that, at each iteration, the R real-valued matrices $\boldsymbol{\Upsilon}_r$ are transformed according to

$$\begin{aligned}\boldsymbol{\Upsilon}_r' &= \boldsymbol{\Theta}_{qp}^T\boldsymbol{\Upsilon}_r\boldsymbol{\Theta}_{qp}\\ &= \begin{bmatrix} v_{11}^{(r)} & \cdots & v_{1p}^{(r)\prime} & \cdots & v_{1q}^{(r)\prime} & \cdots & v_{1d}^{(r)}\\ \vdots & \ddots & \vdots & & \vdots & & \vdots\\ v_{p1}^{(r)\prime} & \cdots & v_{pp}^{(r)\prime} & \cdots & v_{pq}^{(r)\prime} & \cdots & v_{pd}^{(r)\prime}\\ \vdots & & \vdots & \ddots & \vdots & & \vdots\\ v_{q1}^{(r)\prime} & \cdots & v_{qp}^{(r)\prime} & \cdots & v_{qq}^{(r)\prime} & \cdots & v_{qd}^{(r)\prime}\\ \vdots & & \vdots & & \vdots & \ddots & \vdots\\ v_{d1}^{(r)} & \cdots & v_{dp}^{(r)\prime} & \cdots & v_{dq}^{(r)\prime} & \cdots & v_{dd}^{(r)} \end{bmatrix},\\ &\qquad 1\le r\le R.\end{aligned} \tag{18}$$

Here, $v_{k\ell}^{(r)}$ and $v_{k\ell}^{(r)\prime}$ denote the (k,ℓ)-entries of the matrices $\boldsymbol{\Upsilon}_r$ and $\boldsymbol{\Upsilon}_r'$, respectively. Notice that the orthogonal transformation $\boldsymbol{\Theta}_{qp}^T\boldsymbol{\Upsilon}_r$ changes only rows p and q of $\boldsymbol{\Upsilon}_r$, while $\boldsymbol{\Upsilon}_r\boldsymbol{\Theta}_{qp}$ changes only columns p and q of $\boldsymbol{\Upsilon}_r$. Thus, the orthogonal similarity transformation (18) changes only elements of $\boldsymbol{\Upsilon}_r$ that appear in rows and columns p and q as indicated in (18). More specifically, the entries of $\boldsymbol{\Upsilon}_r'$ changed on its strictly lower triangular part $\mathcal{L}(\boldsymbol{\Upsilon}_r')$ are given by

$$\begin{aligned} v_{pk}^{(r)\prime} &= cv_{pk}^{(r)} - sv_{qk}^{(r)}, && 1\le k<p\\ v_{qk}^{(r)\prime} &= sv_{pk}^{(r)} + cv_{qk}^{(r)}, && 1\le k<q, \quad k\ne p\\ v_{qp}^{(r)\prime} &= s[cv_{pp}^{(r)} - sv_{pq}^{(r)}] + c[cv_{qp}^{(r)} - sv_{qq}^{(r)}]\\ v_{kp}^{(r)\prime} &= cv_{kp}^{(r)} - sv_{kq}^{(r)}, && p<k\le d, \quad k\ne q\\ v_{kq}^{(r)\prime} &= sv_{kp}^{(r)} + cv_{kq}^{(r)}, && q<k\le d. \end{aligned}$$

Recall that only $\mathcal{L}(\boldsymbol{\Upsilon}'_r)$ contributes to the cost function (15). Therefore, the change of this cost function can be expressed as

$$\begin{aligned}\Delta\psi(\boldsymbol{\Theta}_{qp}) &= \sum_{r=1}^{R}[\|\mathcal{L}(\boldsymbol{\Upsilon}'_r)\|_{\mathrm{F}}^2 - \|\mathcal{L}(\boldsymbol{\Upsilon}_r)\|_{\mathrm{F}}^2] \\ &= \sum_{r=1}^{R}\left\{ v_{qp}^{(r)\prime 2} + \sum_{k=(p+1)}^{q-1}[v_{qk}^{(r)\prime 2} + v_{kp}^{(r)\prime 2}] \right. \\ &\quad \left. - v_{qp}^{(r)2} - \sum_{k=(p+1)}^{q-1}[v_{qk}^{(r)2} + v_{kp}^{(r)2}] \right\} \qquad (19)\end{aligned}$$

where we have used the fact that

$$v_{pk}^{(r)\prime 2} + v_{qk}^{(r)\prime 2} = v_{pk}^{(r)2} + v_{qk}^{(r)2}, \qquad 1 \le k < p$$

and

$$v_{kp}^{(r)\prime 2} + v_{kq}^{(r)\prime 2} = v_{kp}^{(r)2} + v_{kq}^{(r)2}, \qquad q < k \le d.$$

Differentiating (19) with respect to ϑ, using the abbreviation $t = \tan\vartheta$ which implies $c = \cos\vartheta = 1/\sqrt{1+t^2}$, $s = \sin\vartheta = t/\sqrt{1+t^2}$, and multiplying the result by $(1+t^2)^2/2$ yields the fourth order polynomial

$$p(t) = [1 \quad t \quad t^2 \quad t^3 \quad t^4] \cdot \sum_{r=1}^{R} \boldsymbol{c}^{(r)} \qquad (20)$$

with

$$\begin{aligned}\boldsymbol{c}^{(r)} &= \boldsymbol{c}_{qp}^{(r)} + \sum_{k=(p+1)}^{q-1}\{\boldsymbol{c}_{\mathrm{add}}[v_{pk}^{(r)}, v_{qk}^{(r)}] \\ &\quad - \boldsymbol{c}_{\mathrm{add}}[v_{kp}^{(r)}, v_{kq}^{(r)}]\} \in \mathbb{R}^5,\end{aligned}$$

$$\boldsymbol{c}_{qp}^{(r)} = \begin{bmatrix} v_{qp}^{(r)} \cdot [v_{pp}^{(r)} - v_{qq}^{(r)}] \\ [v_{pp}^{(r)} - v_{qq}^{(r)}]^2 - 2v_{qp}^{(r)} \cdot [v_{pq}^{(r)} + v_{qp}^{(r)}] \\ -3 \cdot [v_{pp}^{(r)} - v_{qq}^{(r)}] \cdot [v_{pq}^{(r)} + v_{qp}^{(r)}] \\ -[v_{pp}^{(r)} - v_{qq}^{(r)}]^2 + 2v_{pq}^{(r)} \cdot [v_{pq}^{(r)} + v_{qp}^{(r)}] \\ v_{pq}^{(r)} \cdot [v_{pp}^{(r)} - v_{qq}^{(r)}] \end{bmatrix}$$

and

$$\boldsymbol{c}_{\mathrm{add}}(a,b) = \begin{bmatrix} a \cdot b \\ a^2 - b^2 \\ 0 \\ a^2 - b^2 \\ -a \cdot b \end{bmatrix}.$$

The critical points of $\Delta\psi(\boldsymbol{\Theta}_{qp})$ in (19) are the roots of the polynomial $p(t)$ in (20). Observe that only the real-valued roots of $p(t)$ yield valid options for the desired orthogonal rotation $\boldsymbol{\Theta}_{qp}$. A real-valued critical point of $\Delta\psi(\boldsymbol{\Theta}_{qp})$ is a minimum if

$$\frac{d}{d\vartheta}\left[\frac{p(\tan\vartheta)}{(1+\tan^2\vartheta)^2}\right] > 0.$$

Straightforward calculations show that this condition is met if

$$\frac{dp(t)}{dt} = c_1 + 2c_2 t + 3c_3 t^2 + 4c_4 t^3 > 0 \qquad (21)$$

$$\text{where } [c_0 c_1 \quad c_2 \quad c_3 \quad c_4]^T = \sum_{r=1}^{R} \boldsymbol{c}^{(r)}$$

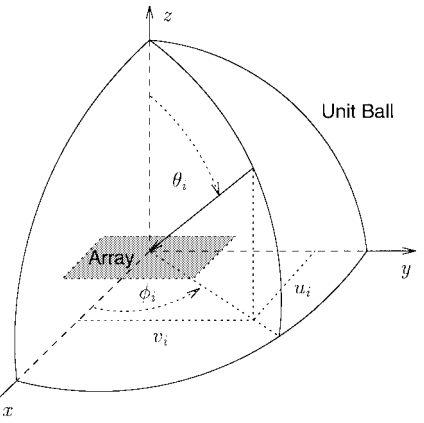

Fig. 1. Definitions of azimuth ($-180° < \phi_i \le 180°$) and elevation ($0° \le \theta_i \le 90°$). The direction cosines u_i and v_i are the rectangular coordinates of the projection of the corresponding point on the unit ball onto the equatorial plane.

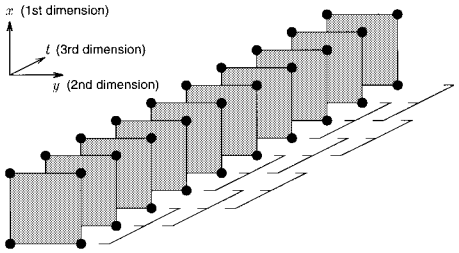

Fig. 2. 3-D Unitary ESPRIT for joint 2-D angle and carrier estimation using a URA of 2×2 elements and $M_3 = 10$ (temporal) snapshots. Temporal smoothing with $L = L_3 = 8$ subarrays, each containing $M_{\mathrm{sub}_3} = M_3 - L_3 + 1 = 3$ snapshots, is performed along the third (temporal) dimension.

and $t = \tan\vartheta$. Notice that there are at most two real-valued roots that satisfy (21). From these possibilities, we choose the value of t (or the corresponding rotation angle ϑ) that minimizes (19). However, we only use the corresponding elementary Jacobi rotation $\boldsymbol{\Theta}_{qp}$ if

$$\Delta\psi(\boldsymbol{\Theta}_{qp}) < 0$$

i.e., the chosen rotation reduces the cost function. Otherwise, no rotation is applied at this particular iteration step. Such a strategy is closely related to the 1-D Jacobi-type methods discussed in [12].

If c_4, the coefficient of t^4 in (20), i.e., the last component of the coefficient vector $\sum_{r=1}^{R} \boldsymbol{c}^{(r)}$, equals zero, $p(t)$ reduces to a third order polynomial. Then $t = \infty$ is also a critical point[4] of $\Delta\psi(\boldsymbol{\Theta}_{qp})$. It corresponds to a valid option for the rotation angle ϑ, i.e., a minimum of $\Delta\psi(\boldsymbol{\Theta}_{qp})$, if $c_3 > 0$.

IV. 3-D Unitary ESPRIT for Joint 2-D Angle and Carrier Estimation

As a 3-D application of the new SSD, consider a URA consisting of $M_1 \times M_2$ identical antennas lying on a rectangular grid in the x–y plane. The interelement spacing in x- and y-

[4]Obviously, $t = \infty$ corresponds to the rotation angle $\vartheta = \pi/2$. Alternatively, one could consider $t = -\infty$. Notice that $t = \infty$ and $t = -\infty$ lead to the same change of the cost function (19).

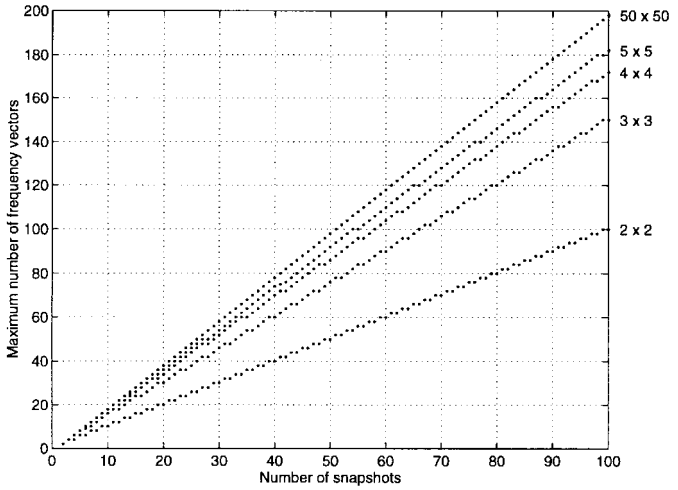

Fig. 3. 3-D Unitary ESPRIT for joint 2-D angle and carrier estimation: Maximum number of frequency vectors $d_{\max}$ as a function of the number of snapshots M_3 for different array sizes $M_1 \times M_2$ if the number of temporal subarrays $L = L_3$ is chosen such that $d_{\max}$ is maximized.

direction will be called Δ_x and Δ_y, respectively. Incident on the array are d narrowband planar wavefronts with speed of propagation c, azimuth ϕ_i, elevation θ_i, and carrier frequency f_i, $1 \le i \le d$. Let $u_i = \cos\phi_i \sin\theta_i$ and $v_i = \sin\phi_i \sin\theta_i$ denote the direction cosines of the ith source relative to the x- and y-axes as illustrated in Fig. 1. For each source, the 2-D angular position and the corresponding carrier frequency have to be estimated simultaneously. If M_3 snapshots are observed at each sensor, 3-D Unitary ESPRIT used in conjunction with the SSD can handle this task. In this case, $N = 1$, and the R =3-D frequency vectors (2) have the components

$$\mu_i^{(1)} = \frac{2\pi f_i}{c}\Delta_x u_i, \quad \mu_i^{(2)} = \frac{2\pi f_i}{c}\Delta_y v_i$$

and

$$\mu_i^{(3)} = 2\pi f_i T_s$$

where T_s denotes the sampling interval. Since only one experiment ($N = 1$) is available, 3-D smoothing as discussed at the end of Section II-B should be used as a preprocessing step. In most applications, it fairly easy to collect a large number of temporal snapshots M_3, whereas increasing the number of sensors in either the x- or the y-direction (M_1 or M_2) would be significantly more expensive. We, therefore, suggest to use smoothing only along the third (the temporal) dimension as illustrated in Fig. 2. Accordingly, M_3 is replaced by $M_{\text{sub}_3} = M_3 - L_3 + 1$, and we can estimate up to

$$d_{\max} = \min\{m_1, m_2, m_3, 2NL\} \tag{22}$$

frequency vectors $\boldsymbol{\mu}_i$, where

$$m_1 = (M_1 - 1)\cdot M_2 \cdot M_{\text{sub}_3},\ m_2 = M_1 \cdot (M_2 - 1)\cdot M_{\text{sub}_3},$$
$$m_3 = M_1 \cdot M_2 \cdot (M_{\text{sub}_3} - 1)$$

and $L = L_3$ is the number of temporal subarrays. In Fig. 3, the maximum number of frequency vectors $d_{\max}$ is plotted as a function of the number of snapshots M_3 if the number of temporal subarrays $L = L_3$ is chosen such that $d_{\max}$ in (22) is maximized. The curves for five different array sizes $M_1 \times M_2$ are shown. Even with a URA of size 2×2, the 2-D arrival angles and carriers of an arbitrary number of wavefronts can be estimated if the window length M_3 (number of used snapshots) is chosen sufficiently large.

Simulations: Simulations were conducted with $d = 4$ wavefronts and the following parameters: $M_1 = 2$, $M_2 = 2$, $M_3 = 10$, $s_i = e^{\mathrm{j}(2\pi i/40)}$, i = 1, 2, 3, 4.

$$\boldsymbol{\mu}_1 = \pi[0.05 \quad -0.5 \quad 0.8]^T, \quad \boldsymbol{\mu}_2 = \pi[0.5 \quad 0.5 \quad 0.8]^T$$
$$\boldsymbol{\mu}_3 = \pi[0.5 \quad 0.5 \quad 0.2]^T, \quad \boldsymbol{\mu}_4 = \pi[0.0 \quad 0.2 \quad 0.2]^T.$$

Temporal smoothing with eight subarrays, each containing three snapshots, was performed along the third (the temporal) dimension, as illustrated in Fig. 2. Therefore, the maximum number of frequency vectors is given by

$$d_{\max} = \min\{m_1, m_2, m_3, 2NL\} = \min\{6, 6, 8, 16\} = 6.$$

In this example, LS was used to solve the real-valued invariance equations (12). As an *ad hoc* alternative to the SSD, we have also computed the eigendecomposition of $\boldsymbol{\Upsilon}_1$ and applied the resulting eigenvectors to $\boldsymbol{\Upsilon}_2$ and $\boldsymbol{\Upsilon}_3$. Let $\hat{\boldsymbol{\mu}}_{i_k} \in \mathbb{R}^3$ denote the estimated frequency vector of the ith source obtained at the kth run. Sample performance statistics were computed from $K = 1000$ independent trials as

$$\text{RMSE}_i = \sqrt{\frac{1}{K}\sum_{k=1}^{K}\left\|\frac{1}{\pi}(\hat{\boldsymbol{\mu}}_{i_k} - \boldsymbol{\mu}_i)\right\|^2}, \qquad i = 1, 2, 3, 4.$$

The resulting RMS errors for sources 1, 2, 3, and 4 are depicted in Fig. 4, which clearly shows that the SSD outperforms the *ad hoc* approach (3-D Unitary ESPRIT without SSD). To illustrate the accuracy of the proposed closed-form algorithm, we have also plotted the conditional (or deterministic) Cramér–Rao lower bound (solid lines). It was calculated via a straightforward 3-D extension of the results presented in [17]. Note that the frequencies of sources 2 and 3 cannot be identified through the *ad hoc* approach (dotted lines), whereas the performance of *3-D Unitary ESPRIT with the SSD* (dashed lines) is very close to the Cramér–Rao bound, except for very low signal-to-noise ratios (SNR's).

Using the same parameters as before, we have also plotted the evolution of the cost function $\psi(\boldsymbol{\Theta})$, defined in (15), for different SNR's (Fig. 5). As expected, the value of the cost function at convergence indicates the strength of the additive noise. Only without additive noise, the three matrices $\boldsymbol{\Upsilon}_r$, $r = 1,2,3$, share precisely the same eigenvectors, and the cost function $\psi(\boldsymbol{\Theta})$ can, therefore, be driven to zero.

V. Concluding Remarks

In this paper, we have extended Unitary ESPRIT to the multidimensional case to solve the multidimensional harmonic

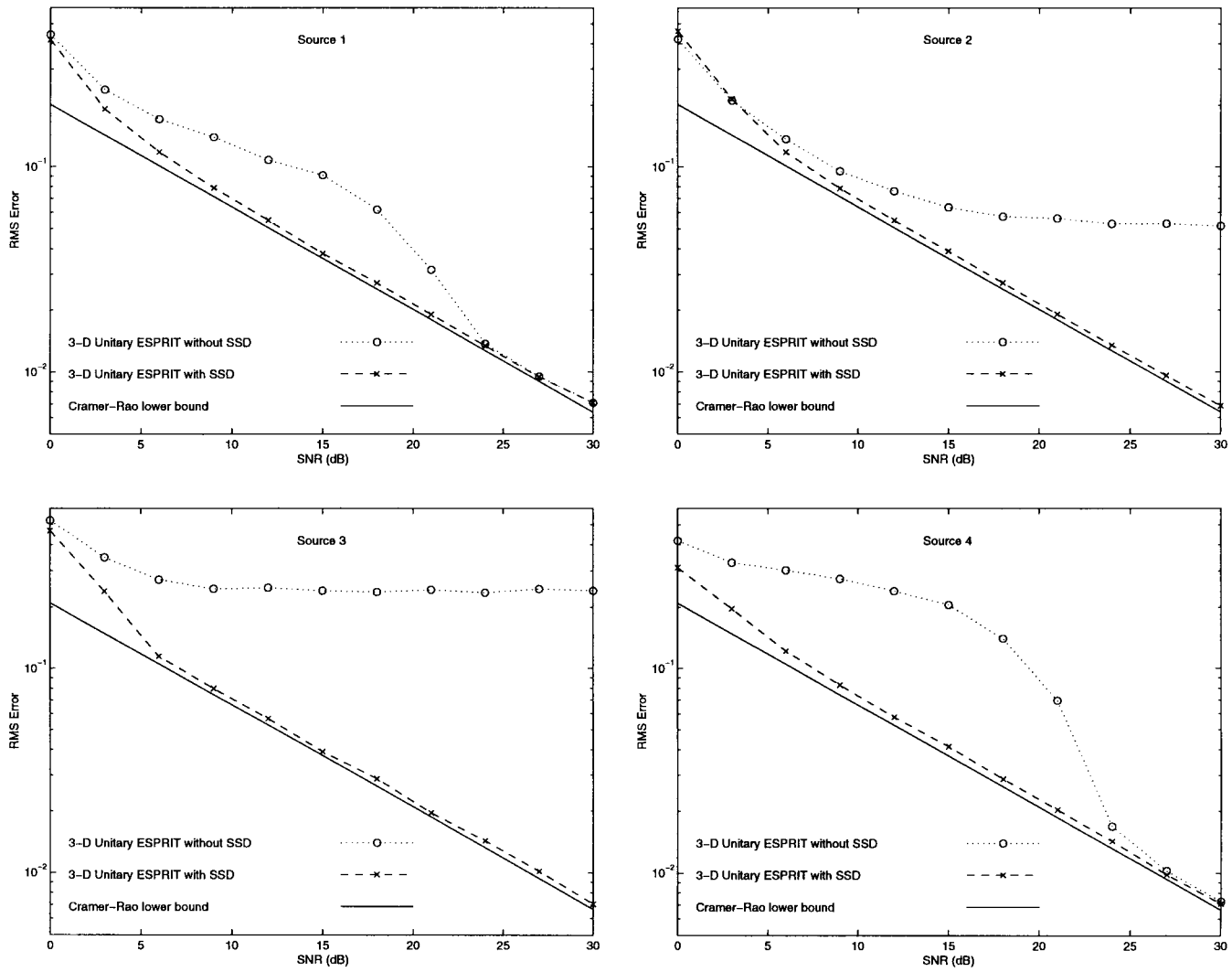

Fig. 4. Comparison of 3-D Unitary ESPRIT with and without the SSD with the Cramér–Rao lower bound (solid lines). Temporal smoothing with $L = L_3 = 8$ subarrays was performed along the third (temporal) dimension ($d = 4$, $R = 3$, $M_1 = 2$, $M_2 = 2$, $M_3 = 10$, $N = 1$, $K = 1000$ trials).

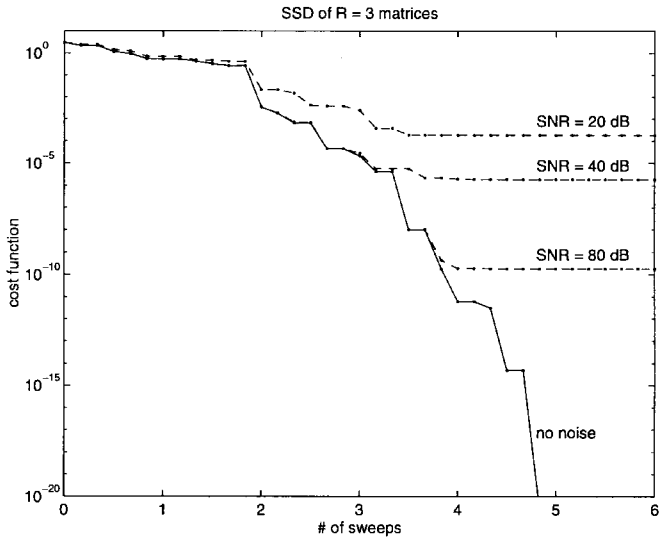

Fig. 5. Evolution of the cost function$\psi(\Theta)$ for different SNR's ($d = 4$, $R = 3$, $M_1 = 2$, $M_2 = 2$, $M_3 = 10$, $N = 1$).

retrieval problem. R-D Unitary ESPRIT is a new closed-form algorithm to estimate several undamped R-dimensional modes (or frequencies) along with their correct pairing from noise-corrupted measurements taken on an R-dimensional grid. Here, the SSD of several real-valued, nonsymmetric matrices reveals their "average eigenstructure" and, thereby, achieves automatic pairing of the estimated R-dimensional modes via a closed-form procedure that neither requires any search nor any other heuristic pairing strategy. Like its 1-D and 2-D counterparts, R-D Unitary ESPRIT inherently includes forward–backward averaging and is efficiently formulated in terms of real-valued computations throughout. In the array processing context, a 3-D extension of Unitary ESPRIT can be used to estimate the 2-D arrival angles and carrier frequencies of several impinging wavefronts simultaneously.

REFERENCES

[1] J. Byrne, D. Cyganski, R. Vaz, and C. R. Wright, "An N-D technique for coherent wave DOA estimation," in *Proc. 7th SP Workshop on Statistical Signal Processing*, Quebec City, P.Q., Canada, June 1994, pp. 425–428.

[2] J. F. Cardoso and A. Souloumiac, "Blind beamforming for non Gaussian signals," *Inst. Elect. Eng. F*, vol. 140, pp. 362–370, Dec. 1993.

[3] ——, "Jacobi angles for simultaneous diagonalization," *SIAM J. Matrix Anal. Appl.*, vol. 17, pp. 161–164, Jan. 1996.
[4] D. Cyganski, R. F. Vaz, and C. R. Wright, "Model-based 3-D object pose estimation from linear image decomposition and direction of arrival estimation," in *Proc. SPIE, Model-Based Vision*, San Diego, CA, July 1992, vol. 1827, pp. 10–18.
[5] G. H. Golub and C. F. van Loan, *Matrix Computations*, 2nd ed. Baltimore, MD: Johns Hopkins Univ. Press, 1989.
[6] M. Haardt, *Efficient One-, Two-, and Multidimensional High-Resolution Array Signal Processing*, J. A. Nossek, Ed. Aachen, Germany: Shaker Verlag, 1996.
[7] ——, "Structured least squares to improve the performance of ESPRIT-type algorithms," *IEEE Trans. Signal Processing*, vol. 45, pp. 792–799, Mar. 1997.
[8] M. Haardt, R. N. Challa, and S. Shamsunder, "Improved bearing and range estimation via high-order subspace based (Unitary ESPRIT)," in *Proc. 30th Asilomar Conf. Signals, Systems, and Computers*, Pacific Grove, CA, Nov. 1996.
[9] M. Haardt and J. A. Nossek, "Unitary ESPRIT: How to obtain increased estimation accuracy with a reduced computational burden," *IEEE Trans. Signal Processing*, vol. 43, pp. 1232–1242, May 1995.
[10] ——, "2-D spatial filters for coherent multipath signals," in *Proc. IEEE/IEE Int. Conf. on Telecommunications*, Apr. 1996, vol. 2, pp. 675–678.
[11] ——, "3-D Unitary ESPRIT for joint 2-D angle and carrier estimation," in *Proc. IEEE Int. Conf. Acoust., Speech, Signal Processing*, Munich, Germany, Apr. 1997, vol. 1, pp. 255–258.
[12] K. Hüper and U. Helmke, "Structure and convergence of Jacobi-type methods," Technical University of Munich, Institute of Network Theory and Circuit Design, Tech. Rep. TUM-LNS-TR-95-2, July 1995, submitted to *Numerische Mathematik*.
[13] A. Lee, "Centrohermitian and skew-centrohermitian matrices," *Linear Algebra Applicat.*, vol. 29, pp. 205–210, 1980.
[14] U. Martin, "Modeling the mobile radio channel by echo estimation," *Frequenz*, vol. 48, pp. 198–212, 1994.
[15] ——, "Echo estimation—Deriving simulation models for the mobile radio channel," in *Proc. IEEE Vehicular Technology Conf.*, Chicago, IL, July 1995, vol. 1, pp. 231–235.
[16] ——, "A directional radio channel model for densely build-up urban area," in *Proc. 2nd Europ. Personal Mobile Communications Conf.*, Bonn, Germany, Sept. 1997, pp. 237–244.
[17] P. Stoica and A. Nehorai, "MUSIC, maximum likelihood, and Cramer–Rao bound," *IEEE Trans. Acoust., Speech, Signal Processing*, vol. 37, pp. 720–741, May 1989.
[18] F. Vanpoucke, "Algorithms and architectures for adaptive array signal processing," Ph.D. dissertation, Katholieke Univ. Leuven, Leuven, Belgium, Feb. 1995.
[19] C. R. Wright, "Multidimensional direction of arrival performance bounds and optimization for nonstationary noise," Ph.D. dissertation, Worcester Polytechnic Inst., Worcester, MA, May 1994.
[20] M. D. Zoltowski, M. Haardt, and C. P. Mathews, "Closed-form 2D angle estimation with rectangular arrays in element space or beamspace via Unitary ESPRIT," *IEEE Trans. Signal Processing*, vol. 44, pp. 316–328, Feb. 1996.

Martin Haardt (S'90–M'98) was born in Germany on October 4, 1967. He received the Dipl.-Ing. (M.S.) degree from the Ruhr-University Bochum, Germany, in 1991, and the Doktor-Ing. (Ph.D.) degree from the Technical University of Munich, Germany, in 1996, both in electrical engineering.

From 1989 to 1990, he was a Visiting Scholar at Purdue University, West Lafayette, IN, sponsored by a fellowship of the German Academic Exchange Service (DAAD). From 1991 to 1993 he worked for Siemens AG, Corporate Research and Development, Munich, conducting research in the areas of image processing and biomedical signal processing. From 1993 to 1996, he was a Research Associate with the Institute of Network Theory and Circuit Design at the Technical University of Munich. Since 1997, he has been with the Siemens Mobile Communications Division, Munich, where he is responsible for strategic research for third generation mobile radio systems. His current research interests include mobile communications, array signal processing, spectral estimation, and numerical linear algebra. He is a contributing author to *The Digital Signal Processing Handbook* (CRC Press and IEEE Press, 1997).

Dr. Haardt received the Rohde & Schwarz Outstanding Dissertation Award for his Ph.D. dissertation on *Efficient One-, Two-, and Multidimensional High-Resolution Array Signal Processing* in 1997.

Josef A. Nossek (S'72–M'74–SM'81–F'93) was born in Vienna, Austria, on December 17, 1947. He received the Dipl.-Ing. and Ph.D. degrees, both in electrical engineering, from the Technical University of Vienna in 1974 and 1980, respectively.

In 1974, he joined Siemens AG, Munich, Germany, where he was engaged in the design of passive and active filters for communication systems. In 1978, he became a Supervisor, and in 1980, head of a group of laboratories concerned with the design of monolithic filters (analog and digital) and electromechanical and microwave filters. In 1982, he became head of a group of laboratories designing digital radio systems within the Transmission Systems Department. In 1985, he spent a month as a Visiting Professor at the University of Capetown, South Africa. From 1987 to 1989, he was head of the Radio Systems Design Department. Since April 1989, he has been a Full Professor and the Head of the Institute of Network Theory and Circuit Design at the Technical University of Munich. He teaches undergraduate and graduate courses in the field of circuit and system theory, and conducts research in the areas of real-time signal processing, neural networks, and dedicated VLSI-architectures. He has published more than 100 papers in scientific and technical journals and conference proceedings, and holds a number of patents.

Dr. Nossek received the ITG Best Paper Award in 1988. From 1991 to 1993, he served as an Associate Editor of the IEEE TRANSACTIONS ON CIRCUITS AND SYSTEMS, PART I, and from 1995 to 1997, he was Editor in Chief. He also served as the technical co-chair of the 1997 IEEE International Conference on Acoustics, Speech, and Signal Processing (ICASSP'97), Munich.